

Troposphere Modeling in a Regional GPS Network

S. Skone and V. Hoyle

Department of Geomatics Engineering, University of Calgary, 2500 University Dr. N.W., T2N 1N4 Calgary, Canada
e-mail: sskone@geomatics.ucalgary.ca Tel: +01-403-220-7589; Fax: +01-403-284-1980

Received: 16 November 2004 / Accepted: 12 July 2005

Abstract. By using a regional network of Global Positioning System (GPS) reference stations, it is possible to recover estimates of the slant wet delay (SWD) to all GPS satellites in view. SWD observations can then be used to model the vertical and horizontal structure of water vapor over a local area, using a tomographic approach. The University of Calgary currently operates a regional GPS real-time network of 14 sites in southern Alberta. This network provides an excellent opportunity to study severe weather conditions (e.g. thunderstorms, hail, and tornados) which develop in the foothills of the Rockies near Calgary. In this paper, a 4-D tomographic water vapor model is tested using the regional GPS network. A field campaign was conducted during July 2003 to derive an extensive set of truth data from radiosonde soundings. Accuracies of tomographic water vapor retrieval techniques are evaluated for 1) using only ground-based GPS input, and 2) using a ground-based GPS solution augmented with vertical wet refractivity profiles derived from radiosondes released within the GPS network. Zenith wet delays (ZWD) are computed for both cases, by integrating through the 4-D tomography predictions, and these values are compared with truth ZWD derived from independent radiosonde measurements. Results indicate that ZWD may be modeled with accuracies at the sub-centimeter level using a ground-based GPS network augmented with vertical profile information. This represents an improvement over the GPS-only approach.

Key words: troposphere, water vapor, tomography, GPS, positioning, atmospheric errors Ionosphere, WADGPS, WAAS

1 Introduction

GPS range observations are derived under the assumption that GPS signals travel at the speed of light (or, equivalently, the index of refraction is equal to one) along the satellite-receiver signal path. For GPS orbits of approximately 20,000 km altitude, the signal must travel through the Earth's ionosphere and neutral atmosphere. In these regions indices of refraction can differ significantly from assumptions, such that range errors arise from signal propagation through the Earth's atmosphere. The range errors induced by the ionosphere are dispersive and 99% of the ionospheric effect may be removed using dual frequency GPS observations (Brunner and Gu, 1991).

Range errors associated with propagation through the neutral atmosphere can be classified as a hydrostatic component and a wet delay. The total delay Δs is related to the neutral refractivity N as follows:

$$\Delta s = \int_{\text{path}} \frac{N}{10^6} ds \quad (1)$$

where N may be expressed as (cf. Ware et al., 1997)

$$N = \underbrace{77.6 \frac{P}{T}}_{\text{hydrostatic}} + \underbrace{3.73 \times 10^5 \frac{e}{T^2}}_{\text{wet}} = N_h + N_w \quad (2)$$

The variable P represents air pressure in millibars, T is the temperature in degrees Kelvin and e is the partial pressure of water vapor in millibars. The variables N_h and N_w represent the hydrostatic and wet refractivities, respectively. The total tropospheric range delay (Equation 1) can therefore be expressed as the sum of both wet and hydrostatic components:

$$\Delta s = \text{SHD} + \text{SWD} \quad (3)$$

where SHD and SWD refer to the slant hydrostatic and slant wet delays, respectively, along the signal path.

Range delays arising from the hydrostatic component (SHD) can be computed with accuracies of a few millimeters using existing models, provided that surface barometric or meteorological data are available (Bevis et al., 1992). By using carrier phase-based differential GPS techniques and removing the hydrostatic component, it is possible to recover estimates of the slant wet delay (SWD) for all satellites in view. Previous research has demonstrated that double difference slant water vapor may be determined with millimeter-level accuracy (translating into better than 1 cm accuracy for SWD), for satellite elevation angles greater than 20 degrees (Ware et al., 1997).

Extensive measurements of SWD may be derived from dense geodetic networks of continuously operating GPS reference stations. The time-varying vertical and horizontal structure of wet refractivity may then be modeled by using the SWD as input observables in a tomographic approach. Flores et al. (2000) have developed a 4-D modeling technique in which the wet refractivity (or functions describing the wet refractivity) is estimated for discrete voxels. Horizontal and vertical smoothing constraints are applied to compensate for undetermined voxels. Perturbations of 3.5 mm/km in vertical profiles are resolved for altitudes below 4 km. Gradinarsky and Jarlemark (2002) have proposed a slightly modified approach, in which wet refractivity values in individual voxels are related via cross-correlation (covariance) information, as opposed to applying smoothing constraints. Results of such studies are promising, and suggest that water vapor fields may be derived with sufficient accuracy for meteorology and precise positioning applications.

2 Background

2.1 Tomography

2.1.1 Measurement model

In the derivations presented here, the following properties are assumed for the wet refractivity N_w :

- 1) Horizontal variations of N_w can be described as a low-order expansion in latitude and longitude.
- 2) Vertical variations of N_w can be described as constant values in discrete layers.

This approach is similar to the voxel algorithms, in that the troposphere is considered to consist of discrete vertical layers. Wet refractivity values for each vertical layer are related in the filtering approach via covariance information. Horizontal variations are estimated using a

functional approach, which is essentially equivalent to the smoothing constraints applied in voxel models.

The slant wet delay is related to the wet refractivity through Equation 1. This expression may be re-written for the slant wet delay component as follows:

$$SWD = 10^{-6} \int_{\text{path}} N_w(\phi, \lambda, h) ds \quad (4)$$

where N_w is a function of latitude (ϕ), longitude (λ) and height (h). In assuming that N_w is constant in a given vertical layer, Equation 4 can be approximated as a summation:

$$SWD = \sum_{j=1}^n N_{wj}(\phi_j, \lambda_j, h_j) ds_j \quad (5)$$

where the troposphere consists of n vertical layers and N_{wj} represents the wet refractivity at the mid-point (ϕ_j, λ_j, h_j) of the ray with length ds_j in layer j . This concept is illustrated in Figure 1. Equation 5 can be further re-written to include the functional relationship describing horizontal variations in N_w :

$$SWD = \sum_{j=1}^n (a_{0j} + a_{1j}\Delta\phi_j + a_{2j}\Delta\lambda_j + a_{3j}\Delta\phi_j^2 + a_{4j}\Delta\lambda_j^2 + a_{5j}\Delta\phi_j\Delta\lambda_j) ds_j \quad (6)$$

where

a_{0j}, \dots, a_{5j} are the expansion coefficients for layer j at height h_j

$$\Delta\phi_j = \phi_j - \phi_0$$

$$\Delta\lambda_j = \lambda_j - \lambda_0$$

(ϕ_0, λ_0) is the expansion point (generally chosen as the centroid of the GPS network)

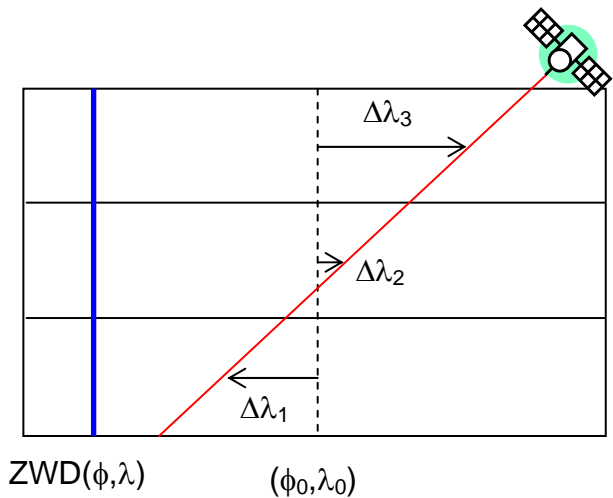


Fig. 1 Sample geometry of wet refractivity estimation in three discrete vertical layers

For the purposes of the testing conducted here, it is assumed that the troposphere consists of eight discrete vertical layers at approximately 750 m intervals. There are a total of 48 unknowns in the adjustment.

2.1.2 System model

The model unknowns (a_{ij} where $i=0,1,\dots,5$ and $j=1,\dots,n$) are approximated as stochastic processes in time. A first order Gauss-Markov process is assumed for temporal correlations in wet refractivity, and the following system model is employed to describe temporal variations in the model coefficients:

$$a_{ij}(t_{k+1}) = e^{-\beta(\Delta t)} a_{ij}(t_k) + w \quad (7)$$

where $1/\beta$ is the *correlation time* and $\Delta t = t_{k+1} - t_k$.

Equation 7 provides a statistical description of how model coefficients vary over time. The coefficients at a given time are only partially correlated with those at later epochs, with the normalized autocorrelation function being given as $e^{-\beta(\Delta t)}$. The uncorrelated part of the predicted coefficient $a_{ij}(t_{k+1})$ is described by a white noise sequence w with variance $q(t)$:

$$q(t) = \sigma^2 [1 - e^{-2\beta(\Delta t)}] \quad (8)$$

where $q(t)$ is the process noise. For the model implemented here, a correlation time Δt of 1800 s is assumed, while the values of σ^2 are set as follows:

$$\begin{aligned} a_0: & \quad \sigma^2 = 10 \text{ (mm/km)}^2 \\ a_1, a_2: & \quad \sigma^2 = 2 \text{ (mm/km)}^2/\text{deg}^2 \\ a_3, a_4, a_5: & \quad \sigma^2 = 0.5 \text{ (mm/km)}^2/\text{deg}^4 \end{aligned}$$

2.1.3 Prediction and update equations

The standard discrete Kalman filter equations are given as follows (after Gelb (1974)), where the superscripts - and + denote prediction and update, respectively.

1) Prediction (from time t_k to t_{k+1})

$$\mathbf{x}^-(t_{k+1}) = \Phi(t_k, t_{k+1})\mathbf{x}^+(t_k) + \mathbf{w} \quad (9)$$

$$\mathbf{P}^-(t_{k+1}) = \Phi(t_k, t_{k+1})\mathbf{P}^+(t_k)\Phi(t_k, t_{k+1}) + \mathbf{Q}(t_k) \quad (10)$$

2) Update (at time t_{k+1})

$$\mathbf{x}^+(t_{k+1}) = \mathbf{x}^-(t_{k+1}) + \mathbf{K}[\mathbf{z}(t_{k+1}) - \mathbf{H}(t_{k+1})\mathbf{x}^-(t_{k+1})] \quad (11)$$

$$\mathbf{P}^+(t_{k+1}) = [\mathbf{I} - \mathbf{K}\mathbf{H}(t_{k+1})]\mathbf{P}^-(t_{k+1}) \quad (12)$$

where \mathbf{K} is the gain matrix:

$$\mathbf{K} = \mathbf{P}^-(t_{k+1})\mathbf{H}^T(t_{k+1})[\mathbf{H}(t_{k+1})\mathbf{P}^-(t_{k+1})\mathbf{H}^T(t_{k+1}) + \mathbf{R}(t_{k+1})]^{-1} \quad (13)$$

The vector \mathbf{x} represents the unknown coefficients (a_{0j}, \dots, a_{5j} for all vertical layers j), Φ is the transition matrix, and \mathbf{H} is the design matrix. The matrices \mathbf{R} and \mathbf{P} are covariance matrices for the observations \mathbf{z} and estimates of the unknowns \mathbf{x} , respectively. Variances for the observations are estimated as follows:

$$\sigma^2 = (1.6\text{cm}^2)/\sin E \quad (14)$$

where E is the satellite elevation angle. The observation variances are based on processing conducted at the University of Calgary, where Bernese software was used to derive SWD observations over a period of several weeks. The SWD estimates were compared with pointed water vapor radiometer observations (truth data) and errors computed for various ranges of elevation angles (Skone and Shrestha, 2003).

The \mathbf{P} matrix is fully populated, where cross-covariances are used to model the correlations between parameters in different vertical layers. The cross-correlation is derived as a function of distance between the given layers. Covariances also depend on height, where lower correlations are assumed for the lower troposphere layers – where inversion events and irregular variations in the vertical wet refractivity profile may occur.

3 Southern Alberta Network and A-GAME

The Southern Alberta Network (SAN) consists of 14 GPS receivers across southern Alberta, deployed in 2003 by the Geomatics Engineering Department at the University of Calgary (Figure 2). The spacing between SAN stations was designed to be approximately 50 km in order to give optimal results for mesoscale numerical weather prediction, and at the same time allow for precise positioning applications. In general, equipment at each SAN station consists of a NovAtel 600 antenna, NovAtel MPC receiver and Paroscientific MET3A meteorological sensor, although some sites do not have a MET3A instruments due to cost limitations.

During July 14-28, 2003 the A-GAME (Alberta – GPS Atmospheric Monitoring Experiment) data collection campaign took place within this network. This campaign was a collaborative effort between the Geomatics Engineering Department at the University of Calgary, the Meteorological Service of Canada (MSC), and Weather Modification Inc. (a private company employed in detection and mitigation of severe weather). Data were collected from the SAN, and radiosondes were released at a number of locations within the network at regular intervals as well as during storm periods.

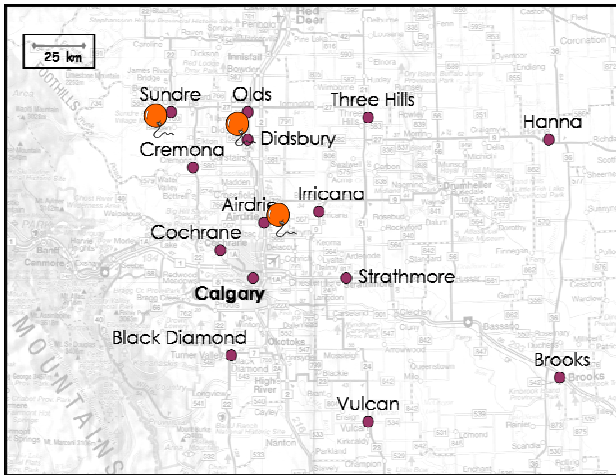


Fig. 2 The Southern Alberta Network during A-GAME 2003. GPS stations are shown as purple dots, and locations of radiosonde launches are shown as orange balloons

The radiosondes were launched at Airdrie approximately three times per day (by personnel from the MSC), and at both Sundre (by personnel from University of Alberta) and Olds/Didsbury airport (by Weather Modification Inc.) once per day - at noon local time. The Sundre radiosonde observations were of questionable quality since the instruments had been stored for some time previously and were tracked visually; these observations were not used to derive results presented in this paper. The Airdrie and Olds/Didsbury instruments were manufactured by Vaisala (2004). In the processing conducted here, radiosonde observations are used as both vertical constraint information (Airdrie) and truth data for assessment of model accuracies (Olds/Didsbury). An example of a single sounding from Airdrie is shown in Figure 3. Weather Modification Inc. also collected radar images within the network (with their TITAN instrument), which allowed correlation of storm evolution with GPS modeling results.

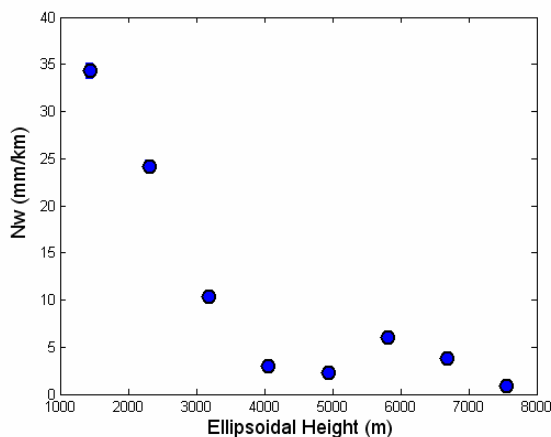


Fig. 3 Sample profile of wet refractivity derived from radiosonde observations at Airdrie

4 Simulation results

A flat network geometry may lead to inaccuracies in vertical profiles of N_w derived using a tomographic approach with only ground-based GPS input. Accuracies of integrated ZWD predictions are compromised to some extent through inability to resolve vertical features. In order to assess such limitations for the SAN, simulations were conducted to evaluate vertical resolution as a function of network geometry. The simulations are based on a suite of MATLAB programs in the Satellite Navigation Toolbox 2.0™ developed by GPSofT. These programs simulate the GPS constellation and range observations for given site coordinates. Slant wet delay observables are generated for the given satellite constellation at various locations in the simulated regional GPS network (network in Figure 2). The tomographic model is then employed (Section 2) to derive refractivity profiles and assess accuracies of model ZWD predictions.

4.1 Method

The approach described in Section 2 is implemented using simulated SWD observations generated every 30 seconds at all reference sites. An elevation cutoff angle of five degrees is assumed, in order to be consistent with further testing conducted in Section 5. Accuracies of the 4-D model were assessed for different tropospheric conditions.

Accuracies of wet refractivity were assessed for two simulated atmospheric profiles:

- 1) Standard profile where N_w decreases smoothly with altitude.
- 2) Inversion event where N_w increases with altitude in the lower troposphere, and decreases with altitude at heights above 2 km.

The simulated SWD values are derived through integration of theoretical N_w along each satellite-receiver line-of-sight (e.g. Equation 1). The focus of these tests is to assess the model capabilities in resolving vertical atmospheric structure. The wet refractivity is therefore assumed to have negligible horizontal variations. The vertical distribution of N_w is simulated using the second term in Equation 2 and the following expressions for water vapor (e) and temperature (T) as a function of height (H):

$$T = T_0 - 6.5H \tag{15}$$

$$e = \frac{U}{100} \exp(-37.2465 + 0.213166T - 0.000256908T^2) \tag{16}$$

where H is in kilometers, T is in Kelvin and e is in millibars. The variable U represents humidity (in percent) and T_0 is the temperature at sea level. For the simulations presented here, U is assumed to be 50 percent and T_0 is 293 °K. The simulated SWD observations have additional random errors imposed as a function of elevation angle, with magnitudes determined from Equation 14. The inversion event is simulated by using Equations 15 and 16 for heights above 2 km, but imposing a positive gradient (as a function of height) in the altitude range 0-2 km.

4.2 Results

Figure 4 shows the wet refractivity estimates generated by the model (after 30 minutes of processing) for the standard profile. The truth data (the N_w profiles used to generate the initial SWD observations) are also plotted for comparison purposes. The N_w values predicted by the model average through the truth profile – representing a smoothed approximation of the vertical atmospheric features. The N_w values are particularly poor at the lower heights, where only one GPS site is located at an altitude sufficiently low enough to observe the bottom atmospheric layer.

Figure 5 shows the wet refractivity estimates for the inversion event (after 30 minutes of processing) versus the truth profile. The irregular inversion profile at lower altitudes is not resolved in the tomography model, with accuracies as poor as 10 mm/km at lower altitudes. Similar to Figure 4, the model values represent a smoothed average of the vertical atmospheric features present above the GPS network. The ground-based GPS observations alone would not allow resolution of inversion profiles.

Results in Figures 4 and 5 demonstrate the impact of network geometry - in particular, vertical station separation within the network - in deriving wet refractivity profiles using ground-based regional networks. Vertical resolution is limited for a flat network such as the SAN, with deficiencies in resolving irregular profiles. For the case of an inversion event, the vertical N_w values generated with a flat network represent only the low-order variations – with an overall smoothing of the true vertical profile.

Results in this section demonstrate that it is difficult to resolve vertical N_w profiles for a flat network geometry, using ground-based GPS data alone. Potential exists, however, to exploit existing sources of vertical information (such as radiosondes or climate models) to constrain the vertical profiles in a tomography approach. By achieving improved vertical resolution through assimilation of such external data sources, it is anticipated that improved ZWD predictions may be derived for GPS

users within the GPS network. This type of approach is explored in the next section.

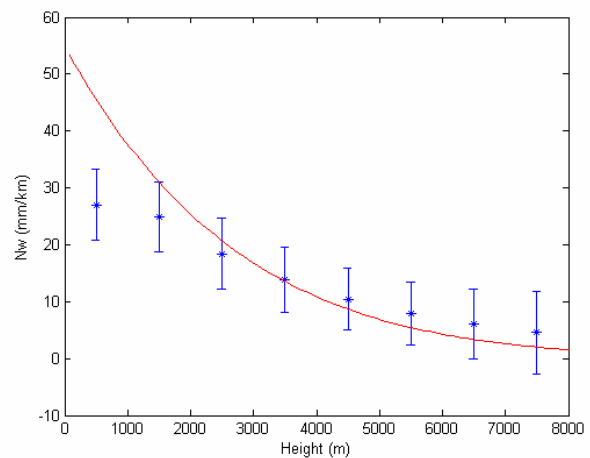


Fig. 4 N_w estimates (blue stars) versus truth (red curve) – standard N_w profile

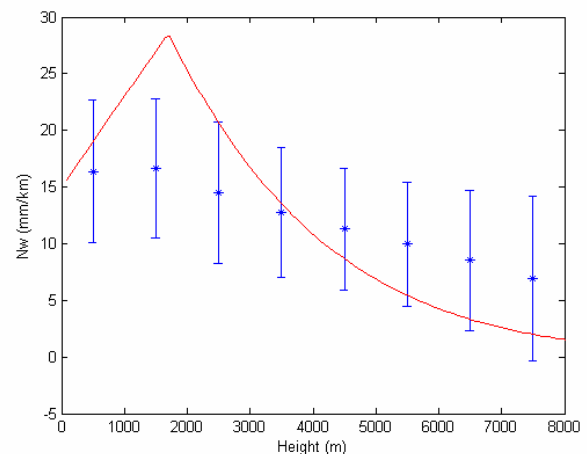


Fig. 5 N_w estimates (blue stars) versus truth (red curve) – inversion event

5 Model results: A-GAME

This section shows model results derived using SAN data, augmented with radiosonde observations, for the A-GAME 2003 campaign. Results are derived for a number of days representing various weather conditions. A brief description of the processing approach and specific data sets follows.

5.1 Estimation of SWD

Hourly estimates of total zenith delays were derived at each receiver in the SAN, with the exception of Olds and Didsbury (Figure 2), using Bernese version 4.2 (Hugentobler et al., 2001), with an ionosphere-free fixed

approach using 30-second observations and an elevation mask of five degrees. The hydrostatic component of the total zenith delay was removed using the Saastamoinen model for hydrostatic delay (cf. Bar-Server and Kroger, 1998):

$$D_H = \frac{0.22765P}{(1 - 0.00266 \cos 2\phi - 0.00028h)} \quad (17)$$

where D_H is the hydrostatic delay in centimeters, P is the pressure at the station in millibars, ϕ is the station latitude in degrees and h is the station height in kilometers. The remaining zenith wet delay was then mapped to the appropriate elevation angle using the Niell wet mapping function (Niell, 1996). In this way, SWD observations were derived for all satellites in view at each available station within the SAN (Figure 2). These observations are used as input observables in the tomography model.

5.2 Radiosonde vertical N_w constraints and truth data

As described in Section 3, radiosonde observations were available at a number of SAN sites during the A-GAME 2003 campaign. These measurements can be used as additional input observations for the tomographic model - serving essentially as vertical profile constraints. The addition of such high-resolution vertical information allows improved 4-D modeling using the tomographic approach, when combined with the SWD estimates from GPS reference sites. For the tests conducted here, two sets of radiosonde observations are used:

- Airdrie: vertical profiles of N_w are derived and assimilated into the tomography model.
- Olds/Didsbury airport: vertical profiles of N_w are derived but excluded from the tomography adjustment and instead used as independent truth data - to assess model prediction accuracies.

Note that Airdrie and Olds/Didsbury airport sites are ~50 km apart. Neither Olds nor Didsbury GPS observations were used in the tomography processing, in order to independently assess model predictions in this region when compared with the local (Olds/Didsbury Airport) radiosonde truth values.

In order to assimilate the Airdrie radiosonde observations into the tomography model, values of wet refractivity were estimated for each sounding. Single observations of N_w were derived from radiosonde measurements for each layer defined in the tomography model (e.g. the eight vertical layers of thickness 750 m), by averaging all N_w point measurements made in the given layer as the balloon ascended. The N_w values were estimated using the following equations from the ICS (2004):

$$\log_{10}(e_s) = \frac{-2937.4}{T} - 4.9283 \log_{10} T + 23.5470 \quad (18)$$

$$e = \frac{\text{RH}(\%)}{100} e_s \quad (19)$$

where

e_s is the saturation pressure of water vapor in hectoPascal or millibars

T is the temperature in Kelvin

e is the water vapor pressure in hectoPascal or millibars

As a final step N_w was calculated from Equation 2 as

$$N_w = 3.73 \times 10^5 \left(\frac{e}{T^2} \right) \quad (20)$$

Observation variances were derived from the laws of error propagation with temperature and relative humidity having uncertainties as given by Vaisala (2004). Wet refractivity profiles and associated error bars were derived for the Airdrie radiosondes in this manner, for direct assimilation into the tomography model. These radiosonde profiles are generally assumed to be valid for a one-hour period, and the analyses presented here focus on periods just after radiosonde launch.

In order to adequately assess the 4-D wet refractivity predictions versus truth, it is important that the Airdrie radiosonde constraint information and the Olds/Didsbury airport radiosonde truth data be available at approximately the same times. Unfortunately, the radiosonde observations at Olds/Didsbury did not always occur at the same time as the radiosonde launches from Airdrie. On the days used for processing, the time differences for these launches were

- July 19, 2003 – same time
- July 20 and 25, 2003 – one hour apart
- July 26, 2003 – two hours apart

5.3 Results and analysis

5.3.1 Data set and processing

Two days were processed as “quiet” days since no meteorological events of interest happened in the network during these times – July 19 and 25, 2003. On July 20 and 26, 2003 large storms passed through the SAN and these times are presented as storm days. As stated earlier, Olds and Didsbury GPS data were excluded from the tomography adjustment since this is where the truth

comparison (model predictions compared with radiosonde truth) takes place.

GPS results shown here are processed using as many stations in the SAN as had surface pressure measurements and GPS data on days of interest. Some data drop-outs were encountered at sites during the A-GAME 2003 campaign, and thus the numbers of stations used for processing were as follows:

- July 19 & 25, 2003 (7 and 8 stations)
- July 20 & 26, 2003 (6 and 5 stations)

In order to retrieve absolute (and not relative) troposphere measurements, three IGS stations were included in the Bernese software processing to derive SWD values: ALGO (Algonquin Park in Ontario, Canada), DRAO (Dominion Radio Astrophysical Observatory in B.C., Canada) and NLIB (North Liberty, U.S.A.) which are approximately 2680 km, 430 km and 1890 km from the network, respectively.

Two types of processing are conducted:

- Ground-based GPS stations alone. In this case, the tomography model uses only SWD input from available GPS stations. This approach is herein referred to as “GPS”.
- The GPS approach is augmented by including radiosonde observations from Airdrie as observational input to the tomography model. This approach is herein referred to as “GPS + RS”.

Wet refractivity and zenith wet delay values are shown in the following sections for times when Olds/Didsbury and Airdrie radiosonde launches took place within enough time of each other for valid model versus truth comparisons to be conducted (two hours or less apart). The ZWD values are derived from the model predictions (for the two different test cases) by integrating upwards through the N_w field predicted by the tomography model at the location of interest (the Olds/Didsbury truth site). Similarly, the Olds/Didsbury N_w truth values are integrated vertically to derive truth ZWD estimates – for comparison with model predictions.

5.3.2 Quiet days

Figures 6 and 7 show results for the first quiet day: July 19, 2003. The results for GPS + RS best match truth for both vertical N_w profiles and integrated ZWD plots. ZWD accuracies of 0.3 cm are achieved for model predictions when radiosonde observations are assimilated into the tomography model, versus accuracies of 2 cm for using ground-based GPS observations alone. The N_w

profile obtained from GPS observations has negative values at the lower altitudes, which is clearly in error.

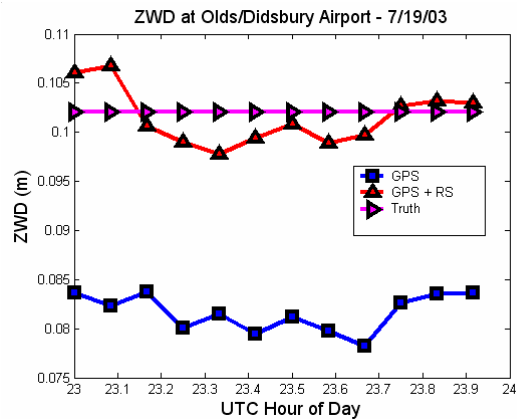


Fig. 6 Integrated ZWD solutions at Olds/Didsbury airport for July 19, 2003

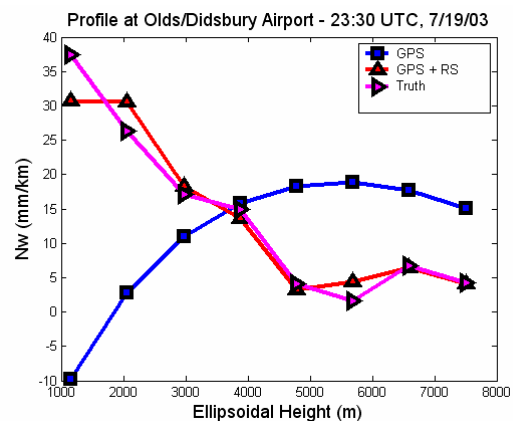


Fig. 7 Vertical N_w profile at Olds/Didsbury airport July 19, 2003 at 23:30 UTC

Integrated ZWD results for July 25 are shown in Figure 8. The GPS + RS solution has an overall accuracy of approximately 1 cm, while the GPS solution has errors of 3 cm. The GPS N_w profile for this day exhibits the correct trend (higher values at lower altitudes) when compared with the July 19 results, but it deviates significantly from the truth values (Figure 9). Overall, results in this section demonstrate the improved modeling of tropospheric wet delay that may be achieved by assimilating vertical profile observations into the tomographic model.

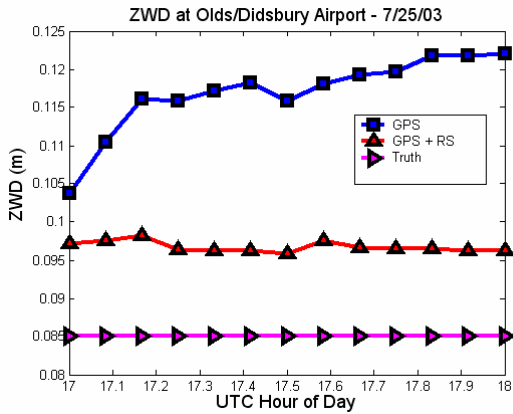


Fig. 8 Integrated ZWD solutions at Olds/Didsbury airport for July 25, 2003

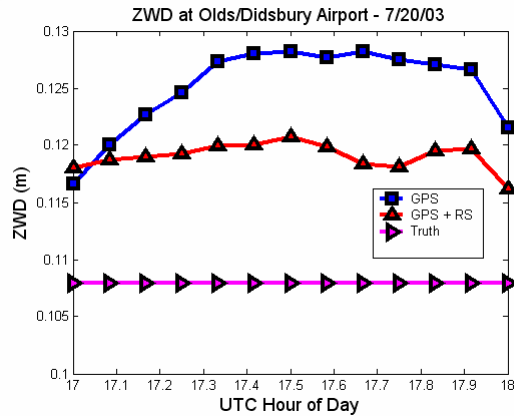


Fig. 10 Integrated ZWD solutions at Olds/Didsbury airport for July 20, 2003

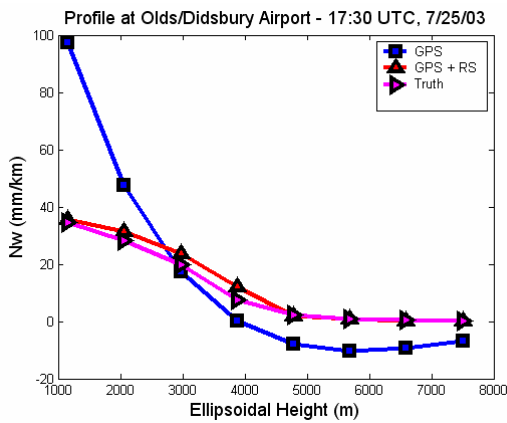


Fig. 9 Vertical N_w profile at Olds/Didsbury airport for July 25, 2003 at 17:30 UTC

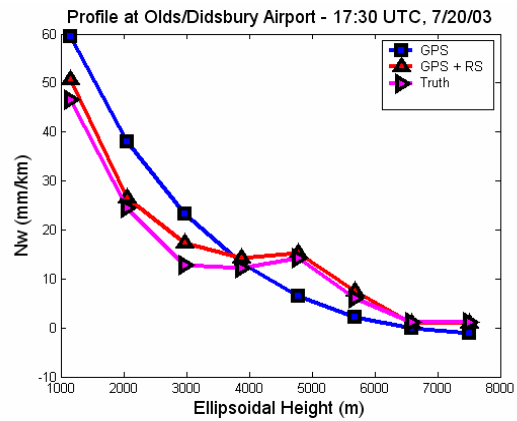


Fig. 11 Vertical N_w profile at Olds/Didsbury airport for July 20, 2003 at 17:30 UTC

5.3.3 Storm days

Figures 10 and 11 show the integrated ZWD values and N_w vertical profiles, respectively, for July 20, 2003. Integrated ZWD values for the GPS + RS solution have improved accuracies (approximately 1 cm) versus the GPS solution. This is consistent with results in Section 5.3.2 for the quiet days. Profiles for July 20 show small-scale variation in the GPS + RS and truth vertical profiles. These features, which appear to be real, are smoothed through in the GPS and GPS solutions.

Figures 12 and 13 show the integrated ZWD values and N_w vertical profiles, respectively, for July 26, 2003. The GPS + RS solution has overall accuracies of approximately 0.5 cm with respect to the truth solution, while the GPS ZWD solutions are approximately 2 cm higher than truth. Again, ZWD results are improved by including radiosonde information in the tomography solution. The GPS N_w profile appears to (incorrectly) represent an inversion structure, while the GPS + RS N_w profile follows the truth profile more closely.

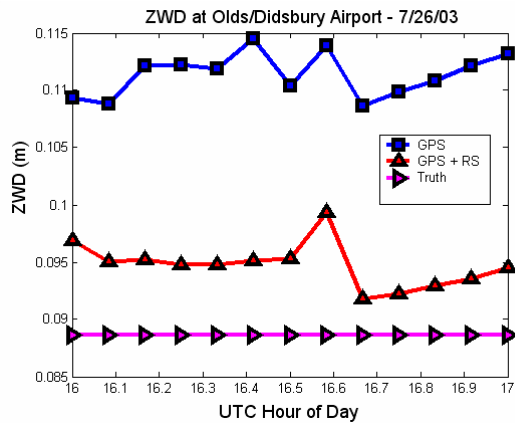


Fig. 12 Integrated ZWD solutions at Olds/Didsbury airport for July 26, 2003

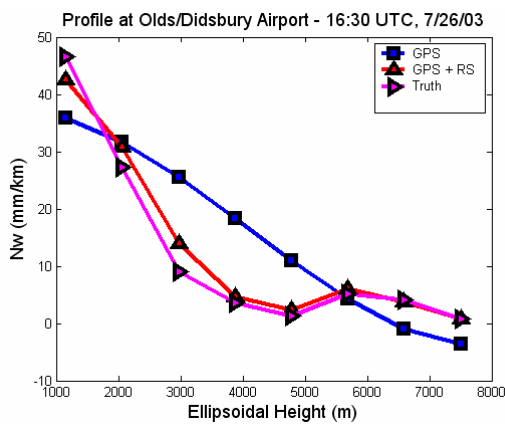


Fig. 13 Vertical N_w profile at Olds/Didsbury airport for July 26, 2003 at 16:30 UTC

5.3.4 Summary

Table 1 summarizes the integrated ZWD results for all cases presented in Sections 5.3.2 and 5.3.3. Accuracies on the quiet day July 25 are the most significantly improved by assimilating radiosonde observations into the tomography model. Overall, the results show promising potential for exploiting ground-based GPS networks and available radiosonde data to model ZWD with cm-level accuracy.

Note that the model ZWD accuracies are perhaps better than expected for the GPS (without radiosonde) solutions, given the poor vertical resolution of the model (e.g. the GPS N_w profile in Figure 7). The tomography N_w solutions are non-unique, however – such that identical integrated quantities may be derived from significantly different N_w profiles. It is possible to derive accurate integrated ZWD estimates from apparently non-realistic vertical N_w profiles. The addition of vertical profile constraints does, however, improve both the model N_w profiles and ZWD predictions.

Tab. 1 Zenith wet delay accuracies from tomography model during times where radiosonde observations are available (storm days in italics)

Date/Time	RMS (CM)	
	GPS	GPS+RS
July 19	2.0	0.3
<i>July 20</i>	1.8	1.1
July 25	3.2	1.2
<i>July 26</i>	2.3	0.6

6 Conclusions

Resolving vertical structures of water vapor using data from a flat GPS network (e.g. the SAN) alone, using a tomography approach, results in poor vertical resolution of wet refractivity, although integrated ZWD quantities are accurate to approximately 1-3 cm. By exploiting other sources of vertical profile information, improvements may be made in tomographic modeling of wet refractivity. Potential sources of vertical profile information include radiosonde data, climate models, microwave profilers, and radio occultation estimates. The addition of radiosonde point measurements from a location within the GPS network (GPS + RS) to ground-based GPS tomography improves the integrated ZWD solution by at least 0.7 cm when compared to the GPS-only tomographic solution, and improves the vertical wet refractivity profiles derived from the tomography model. Absolute ZWD accuracies, when compared to truth values, are in the range 0.3-1.2 cm for both quiet and storm conditions, for this augmented approach.

Water vapor profiles can also be derived from radio occultations using low Earth orbiting (LEO) satellites. Currently several LEO satellites exist with GPS payloads (e.g. CHALLENGING Minisatellite Payload – CHAMP, Satellite de Aplicaciones Cientificas C – SAC-C) and there are plans in place for a six-satellite system in the near future (Constellation Observing System for Meteorology, Ionosphere and Climate – COSMIC). First results from the CHAMP mission have indicated that vertical profiles of humidity agree well with European Centre for Medium-Range Weather Forecast (ECMWF) and National Centers for Environmental Prediction (NCEP) specific humidity data (Wickert et al., 2001) to about 1.5 kilometers above the surface of the Earth, where atmospheric water vapor and multipath degrade the solution (Gregorius and Blewitt, 1998). Since occultation data is likely to become more readily accessible and timely in the future, these measurements could be assimilated into the tomographic estimation routine described in this paper. Future plans for follow-on work in fact include assimilation of N_w profiles derived from radio occultations into the tomography model, and to

determine their benefit for flat GPS network wet refractivity tomography.

Acknowledgements

The authors wish to acknowledge the International GPS Service, for orbit products and raw station data used in the Bernese processing. We acknowledge our collaborators: Craig Smith for formatting of radiosonde observations; and Geoff Strong and Terry Krauss for consultation on meteorological phenomena. Rinske van Gosliga is acknowledged for Bernese processing of A-GAME 2003 data. This work has been funded in part by the Canadian Foundation for Climate and Atmospheric Sciences (CFCAS). Portions of this paper have also been submitted for publication in Proceedings of the ION GNSS 2004 conference.

References

- Bar-Sever Y E.; Kroger P M. (1998): *Estimating horizontal gradients of tropospheric path delay with a single GPS receiver*, Journal of Geophysical Research, 103(B3):5019-5035
- Bevis M S.; Businger S.; Herring T A.; Rocken C.; Anthes R A.; Ware R H. (1992): *GPS meteorology: remote sensing of atmospheric water vapor using the Global Positioning System*, Journal of Geophysical Research, 97(D14):15787-15801
- Braun J.; Rocken C. (2003): *Water vapor tomography within the planetary boundary layer using GPS*, International Workshop on GPS Meteorology, Tsukuba, Japan, 14-17 January, http://dbx.cr.chiba-u.jp/Gps_Met/gpsmet
- Brunner F K.; Gu M. (1991): *An improved model for the dual frequency ionospheric correction of GPS observations*, Manuscripta Geodaetica, 16:205-214
- Flores A.; Ruffini G.; Ruis A. (2000): *4D tropospheric tomography using GPS slant wet delays*, Annales Geophysicae, 18:223-234
- Gelb A. (1974): *Applied Optimal Estimation*, Cambridge, Mass.: MIT Press
- Gradinarsky L.; Jarlemark P. (2002): *GPS tomography using the permanent network in Goteborg: simulations*, Proceedings of IEEE Positioning, Location and Navigation Symposium, Palm Springs, CA, 15-18 April, 128-133
- Gregorius T.; Blewitt G. (1998): *The effect of weather fronts on GPS measurements*, GPS World, May:52-60
- Hugentobler U.; Schaer S.; Fridez P. (2001): *Bernese GPS Software Version 4.2 Manual*, Astronomical Institute University of Berne, February
- Institute of Information and Computing Science (ICS) Web Site (2004), *Temp, humidity and dew-point ONA*, <http://www.cs.uu.nl/wais/html/na-dir/meteorology/temp-dewpoint.html>, Accessed: August 10
- Niell A E. (1996): *Global mapping functions for the atmosphere delay at radio wavelengths*, Journal of Geophysical Research, 101(B2):3227-3246
- Skone S.; Shrestha S. (2003): *4-D modeling of water vapor using a regional GPS network*, Proceedings of the ION National Technical Meeting, Anaheim, CA, 22-24 January
- Vaisala (2004): *RS80 Spec Sheet*, http://www.vaisala.com/DynaGen_Attachments/Att2743/2743.pdf, Accessed August 13
- Ware R.; Alber C.; Rocken C.; Solheim F. (1997): *Sensing integrated water vapour along GPS ray paths*, Geophysical Research Letters, 24:417-420
- Wickert J.; Reigber C.; Beyerle G.; König R.; Marquardt C.; Schmidt T.; Grunwaldt L.; Galas R.; Meehan T.; Melbourne W.; Hocke K (2001): *Atmosphere sounding by GPS radio occultation: first results from CHAMP*, Geophysical Research Letters, 28:3263-3266